Physical Science International Journal

25(2): 26-36, 2021; Article no.PSIJ.68465
ISSN: 2348-0130

The Case Studies of PtX_2 (X = As, P) as High Thermo-power Materials

Adewumi I. Popoola[1*] and Adebayo T. Adepoju[2]

[1]Department of Physics, Federal University of Technology, PMB 704 Akure, Nigeria.
[2]Department of Physics, Federal University of Agriculture, PMB 2373 Markudi, Nigeria.

Authors' contributions

This work was carried out in collaboration between both authors. Author AIP designed the study, performed the calculations and wrote the first draft of the manuscript. Author ATA performed the statistical analysis. Both author read and approved the final manuscript.

Article Information

DOI: 10.9734/PSIJ/2021/v25i230242
Editor(s):
(1) Dr. Lei Zhang, Winston-Salem State University, USA.
(2) Dr. Roberto Oscar Aquilano, University of Rosario (UNR), Argentina.
Reviewers:
(1) Eddwi Hesky Hasdeo, University of Luxembourg, Luxembourg.
(2) Vipul Srivastava, Lovely Professional University, India.
(3) Subhranshu Sekhar Sahu, National Institute of Technology Raipur, India.
Complete Peer review History: http://www.sdiarticle4.com/review-history/68465

Short Research Article

Received 15 March 2021
Accepted 22 May 2021
Published 03 June 2021

ABSTRACT

For thermoelectric applications, semiconductors are generally better than metals and insulators. $PtAs_2$ and PtP_2 are indirect energy gap semiconductors that have been predicted with high thermo-powers (PtP_2 having higher thermopower than $PtAs_2$). The crystal structure and the electronic structure of $PtAs_2$ and PtP_2 are similar except for the energy band gap of PtP_2 that is wider than that of $PtAs_2$. The generalized gradient approximation of the Density Functional Theory (DFT), the Density Functional Perturbation Theory (DFPT) were used to explore the full elastic tensors, phonon dispersion and the thermodynamics of PtP_2 and $PtAs_2$. This was done to understand the link, if any, between high thermo-power materials and the results. The two compounds are dynamically and elastically stable with higher mechanical properties recorded for PtP_2 over $PtAs_2$. The calculated entropy, vibration free energy and the heat capacity at constant volume for $PtAs_2$ (PtP_2) were 354.51 (264.18) J/K; -9.21 (27.84) *k*J and 276.04 (250.36) J/K at 300 K respectively. The low frequency acoustic modes are between 100 - 170 cm^{-1} for $PtAs_2$ while it is between100 - 190 cm^{-1} for PtP_2. The calculated high frequency transverse optical (TO) mode for PtP_2 is 410 cm^{-1} while it is 250 cm^{-1} for $PtAs_2$. Further analysis of the phonons spectrum showed that additional

**Corresponding author: E-mail: ispopoola71@gmail.com, aipopoola@futa.edu.ng;*

bond-bending modes can be created in PtP_2 than in $PtAs_2$. All the results points toward PtP_2 as better material over $PtAs_2$ for thermoelectric application and these, with or without the knowledge of the energy bandgap can serve to guide material selection/modelling.

Keywords: Elastic; vibrational; thermodynamic; DFT; stability; band gap; phonon.

1. INTRODUCTION

The fossil fuel is the primary global energy sources. Its reserves are undergoing depletion daily due to industrialization and population explosion that has placed unprecedented demand on its use. Although, the use of fossil fuels may continue for the next decades, their negative impact such as the emission of the greenhouse gases which has resulted in serious health challenges and climate change has spurred the scientific community into exploring other energy generating technologies that are economically viable with no harmful emissions. The impact of climate change alone is staggering - acid rains, increase in soil erosion, increase in harmful levels of atmospheric ultraviolet radiation and decrease in biodiversity among others [1]. Getting alternative methods of generating, conserving and utilizing clean energy resources may not only in the future prevent economic collapse; it could salvage us from environmental catastrophes and wars [2]. As part of efforts to replace fossil fuels, energy generation from alternative sources such as solar, water, wind and geothermal have received attention.

Thermoelectric (TE) materials are materials in which temperature/voltage gradient can create special effects such as the Seebeck, the Peltier or Thomson's effect [3]. The Seebeck effect occurs when a voltage is generated due to the exposure of TE material to temperature gradient. The Peltier effect occur when temperature is induced in the material as a result of voltage gradients, while the Thomson's effect shows the relationship that exist between the reversible thermal gradient and the electric field in the material. Through TE materials, wasted heat can be easily converted to electricity, making it a possible solution to human energy needs. TE materials have been utilized in waste heat recovery in automobiles [4-5], potable refrigerators [6-8], thermoelectric air conditioning [8-10] and more. A good thermoelectric material should have high efficiency (alternatively call the "figure of merit") and wide operational temperature range. Compared to metals and insulators, semiconductors are generally better TE materials due to their moderate Seebeck coefficients, good electrical conductivity and low thermal conductivity [11-13]. The efficiency of any thermoelectric material is given by the figure of merit (ZT). The figure of merit is a dimensionless quantity that can be expressed as:

$$\mathrm{ZT} = \frac{\mathrm{PT}}{\kappa}, \tag{1}$$

where $P = S^2\sigma$ is the power factor, S, T, σ and κ are the Seebeck coefficient, the temperature, the electrical and thermal conductivities respectively. For higher/improved efficiency, the prospective thermoelectric material must have large Seebeck coefficient (S), large electrical conductivity (σ), and low thermal conductivity. All these are difficult to achieve altogether because materials with large Seebeck coefficient have small conductivity and vice-versa and this have made the discovery of exceptionally performing thermoelectric materials a challenging task. One of the suggested ways to overcome this problem is to develop materials with peculiar band-structure (referred to as the "pudding mold") type, which consists of a dispersive portion and a flat portion [14]. A typical material in which this type of band had justified predicted large S (≈100 μV/K) and power factor (≈50 μW/cmK^2) is the Na_xCoO_2 thermoelectric oxide [15-17]. Compared with the classic thermoelectric material Bi_2Te_3 (which has a power factor of ≈40 μW/cmK^2), other materials in which the "pudding mold" type band is believed to have positively impacted the power factor have been reported [18-20]. Aside the characteristics of the band-structure, the S is believed to increase with the energy band gap at high temperatures.

Interestingly, the pudding mold type band-structure has been reported in some pyrite-type platinum group metal dipnictides such as $PtAs_2$ and PtP_2 [21]. The dipnictides are of interest due to their chemical inertness, good thermal and electronic conductivities [22-23]. They are also known to exhibit high electro-catalytic activity for fuel-cell applications [24-26]. From the aspect of vibrational frequencies and electronic structures, $PtAs_2$ had received more attention than PtP_2. Due largely to lack of experimental data, much of any analysis can for now be done in comparison

with available theoretical data. The predicted energy band gap for $PtAs_2$ is in the range 0.285 - 1.27 eV and that for PtP_2 is in the range of 1.126 - 1.46 eV respectively [21,27-28]. The band gap and the Debye temperature in $PtAs_2$ had been predicted to increase monotonically under increased pressure [29]. For their proposal as optimum thermoelectric materials, Mori et al. [21] had predicted a monotonic increase in the Seebeck coefficient of $PtAs_2$ and PtP_2 with increase in temperature. At the same doping levels, the power factor of PtP_2 has been predicted much higher than for $PtAs_2$ [21]. Ricci et al [30] have also shown that a hole-doped PtP_2 will have a Seebeck value of 532.178 μV/K compared with 124.333 μV/K for $PtAs_2$ over same temperature range. When doped with electrons, the Seebeck coefficient can get as high as -431.449 μV/K for PtP_2 and 86.2044 μV/K for $PtAs_2$. The crystal structure and the band structures of $PtAs_2$ and PtP_2 are similar, except for the energy band gap of PtP_2 that is wider than that of $PtAs_2$. Can energy band gaps be solely responsible for the apparently difference in the transport properties?

The transport properties are not going to be re-investigated as that has been done elsewhere. However, this paper seeks to investigate such other pertinent properties as the elastic constants, phonon dispersion frequencies and the thermodynamic properties. Considering these results together with data available in the literature should enable one have better understanding of the role of all indicators towards optimum performance of thermoelectric materials. The overview of the methodology used in the computation is given in sect. 2. The results of the calculation alongside relevant discussion are given in sect. 3. The work done is finally summarized in sect. 4.

2. CALCULATION METHODS

The crystal structure for $PtAs_2$ and PtP_2 is given in Fig. 1. The structure is of pyrite form. Its Strukturbericht designation is *C*2, with a Pearson symbol of *c*P12. The four metal atoms are located at 4(a) positions, while the eight arsenic (or phosphorus) atoms are in the 8(c) positions.

The first step in any ab initio calculation is optimization. This step was necessary to obtain optimum calculation criteria and lattice geometry. It was done by sampling the potential energy surface repeatedly until a minimum force was achieved. All calculations, leading to the results discussed in this paper were carried out using Quantum Espresso (QE). QE [32] uses plane waves plus pseudo potential to solve the Kohn-Sham of the Density Functional Theory. The electron exchange correlation within the DFT equation was treated using the generalized gradient approximations of Perdew-Burke-Ernzerhof [33]. A total of 1000 k-points (10 × 10 × 10) according to the shifted Monkhorst-Pack scheme [34] and energy cutoff of 40 Rydberg led to convergence in energy (*E*) that was less than 1 meV/atom.

After geometry optimizations, the next was the elastic constants calculation. Mechanical properties depend primarily on the elastic constants. It describes the response of the material to external forces. For cubic lattices such as $PtAs_2$ and PtP_2, only three elastic constants (c_{11} , c_{12} c_{44}), are needed to fully describe the mechanical properties. The procedures followed to obtain these elastic constants are as follows [35]. A strain was applied to each crystal and the energy versus the strain was measured, with the elastic constant determined from the curvature of this function at zero strain. The first set of elastic constant combination (given in eq. 1) was obtained from the bulk modulus $B(V)$ through a fit of energy-volume data to an equation of state.

$$\mathrm{B(V)} = \mathrm{VE^{''}(V)} = \frac{\mathrm{C_{11}+2C_{12}}}{3}, \qquad (2)$$

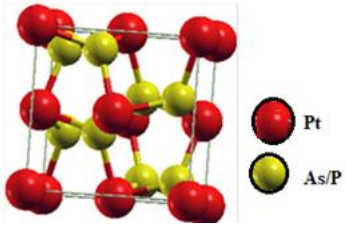

Fig. 1. Crystal structure of $PtAs_2$ and PtP_2. The space group is $Pa\bar{3}$ (no. 205). Structure drawn with XCrySDen [31]

where *V* is the unit cell volume. The second set of the elastic constant combination can be obtained by keeping the unit volume length fixed along the (0 0 1) direction and apply strain in the (1 0 0) direction, while the (0 1 0) direction is simultaneously compressed to conserve the volume. With the fractional change maintained only in the (1 0 0) direction, the following expression is valid:

$$c_{11} - c_{12} = \frac{E''(0)}{V}, \quad (3)$$

V is the volume of the unit cell and *E*(0) is the energy of the unstrained lattice at volume V. To obtain c_{44}, the crystal can be strained in the (1 1 0) direction while simultaneously fixing the volume by compressing in the (1 1 0) direction. The equation defining this setup is:

$$c_{44} = 2\frac{E''(0)}{V}. \quad (4)$$

After determining the independent elastic constants (c_{11}, c_{12} c_{44}), other elastic properties such as the bulk modulus (*B*), shear modulus (*G*), Young's modulus (*E*) and Poisson's ratio (*v*) among others were calculated using the Voight-Reuss-Hill averaging methods [36]. The expressions for all elastic constant dependent properties calculated are given in eq. 5 through eq. 15.

$$c_{11} - c_{12} > 0;\ c_{11} + 2c_{12} > 0;\ c_{44} > 0, \quad (5)$$

$$B = \frac{C_{11}+2C_{12}}{3}, \quad (6)$$

$$G_R = \frac{5(C_{11}-C_{12})C_{44}}{[4C_{44}+3(C_{11}-C_{12})]}, \quad (7)$$

$$G_V = \frac{C_{11}-C_{12}+3C_{44}}{5}, \quad (8)$$

$$G = \frac{G_R+G_V}{2}, \quad (9)$$

$$E = \frac{9BG}{3B+G}, \quad (10)$$

$$v = \frac{3B-2G}{2(3B+G)}, \quad (11)$$

$$A = \frac{2C_{44}}{C_{11}-C_{12}}, \quad (12)$$

$$\zeta = \frac{C_{11}+8C_{12}}{7C_{11}+2C_{12}}, \quad (13)$$

$$H_V = 2\left(\frac{G^3}{B}\right)^{0.585} - 3, \quad (14)$$

$$v_l = \sqrt{\frac{1}{3\rho}[3B + 4G]};\ v_t = \sqrt{\frac{G}{\rho}};$$
$$v_m = \left[\frac{1}{3}\left(\frac{2}{v_t^3} + \frac{1}{v_l^3}\right)\right]^{-1/3};\ \Theta_D = \frac{\hbar}{k_B}\left[\frac{3n}{4\pi}\left(\frac{N_A\rho}{M}\right)\right]^{1/3} v_m, \quad (15)$$

where *A*, is the Zener anisotropy factor [37], ζ, is the Kleinman parameter [38], H_V, is the Vickers hardness index [39], v_l, v_t, and v_m are the magnitude of velocity due to longitudinal waves, transverse waves as well as the average velocity [40]. The Debye temperature (Θ_D) is also a function of the Boltzmann constant (k_B), the Plank constant ($\hbar$), the number of atoms per formula unit (*n*), N_A is the Avogadro constant, ρ is the density of the material and M is the molecular weight.

The phonon band structures and other related thermodynamic properties were calculated using the Density Functional Perturbation Theory (DFPT) [41]. The vibration free energy (*F*) can be derived from phonon calculations. It was achievable using the Quasi-Harmonic-Approximation (QHA). The free energy for any system at a particular temperature *T*, can be expressed as:

$$F(V_P, T) = E(V) + F_{vib}(V, T), \quad (16)$$

with;

$$F_{vib} = k_B T \int_0^\infty \ln\left\{2\sinh\frac{\eta\omega}{2k_B T}\right\} g(\omega)d(\omega), \quad (17)$$

where *E* is the total energy of the system at 0 K and F_{vib} is the vibrational contribution to the vibration free energy. k_B is the Boltzmann constant, ω is the phonon frequencies, $g(\omega)$ is the phonon density of states with $\int_0^\infty g(\omega)d(\omega)$ = 3N, with N being the number of atoms per formula unit. After obtaining the vibration free energy, the entropy (S), internal energy (E) and the heat capacity at constant volume (C_V) can be derived using the following thermodynamic relations:

$$S = -\left(\partial F/\partial T\right)_V\ ;\ E = F + TS\ ;\quad C_V = -T\left(\partial^2 F/\partial^2 T\right)_V \quad (18)$$

3. RESULTS AND DISCUSSION

3.1 Elastic Properties

Since the elastic, vibration and the thermodynamic properties of a material depend on the electronic structure, the calculated electronic structure (density of states and band-structure) for $PtAs_2$ and PtP_2 are presented in

Fig. 2. According to Fig. 2(a) and (c), it is clear that both compounds would exhibit indirect energy band-gap. The peculiar structure, where a band spills to the Fermi level E_F (Fermi level indicated by red line on the plots) between the X and GAMMA (Γ) point in the Brillouin zones is evident for both compounds (see Fig. 2(a) & (c)). The energy band-gap for $PtAs_2$ is narrower around E_F compared with that of PtP_2 which is wider (see Fig. 2(b) & (d)), consistent with the information available in the literatures.

The calculated independent elastic constants (c_{11} , c_{12} , c_{44}) as well as elastic constant dependent properties such as the bulk (*B*), shear (*G*) and Young's modulus (*E*), Frantsevich's ratio (*G*/*B*), Zener anisotropy factor (*A*), Kleinman internal-displacement parameter (ζ), Poisson's ratio (v), sound velocity (v_m), the Debye temperature (Θ_D) as well as the Vicker's hardness index (H_v) are presented in Table 1. There are no available experimental data for comparison. It is evident that the calculated elastic constant results (c_{11}, c_{12} , c_{44}) are in good agreement with other theoretical results (see Table 1). Both PtP_2 and $PtAs_2$ were found to have satisfied the Born–Huang criterion (eq. 5) at ambient condition [42]. The calculated result for *B, G* and *E* are in good agreement with the other reported theoretical results. The elastic constants as well as their dependent properties (*B, G*, *E, v,* v_m, Θ_D and H_v) are higher for PtP_2 than $PtAs_2$. While both compounds ($PtAs_2$ and PtP_2) have same pyrite-type cubic structure, the differences in the sound velocities (v_t, v_l, v_m) and Θ_D between PtP_2 and $PtAs_2$ can be associated with the smaller average atomic mass of phosphorus (30.97) as compared to arsenic (74.92) where according to eq. 15, Θ_D and atomic mass are inversely proportional to each other.

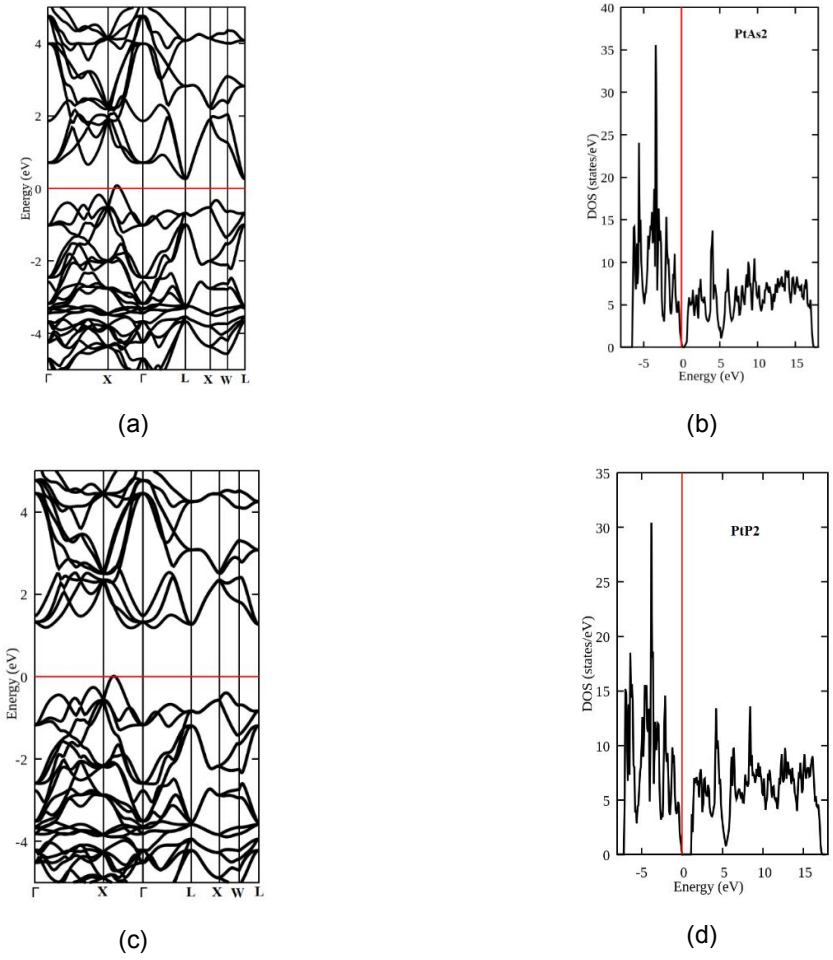

Fig. 2. Calculated band-structure; (a) for $PtAs_2$; (b) density of states for $PtAs_2$; (c) band-structure for PtP_2; (d) density of states for PtP_2

Table 1. Calculated isotropic bulk modulus *B*, shear modulus *G*, Young's modulus *E*, Frantsevich's ratio (*G*/*B*), elastic constants (c_{11}, c_{12}, c_{44}), Zener anisotropy factor *A*, Kleinman parameter ζ, Poisson's ratio v, Vicker's hardness index H_v, sound velocities (v_t, v_l, v_m), and the Debye temperature Θ_D, for $PtAs_2$ and PtP_2. Results from other sources are in brackets

Properties	$PtAs_2$	PtP_2
B (GPa)	169.00 [152][a], [136][b], [163.4][c]	178.99 [177][d]
G (GPa)	89.95 [86][a], [83][d]	103.22 [117][d]
G/*B*	0.53	0.58
E (GPa)	229.12 [216][a]	259.57
c_{11} (GPa)	344.41 [307][a], [290.3][b], [341.9][c]	393.86 [399][d]
c_{12} (GPa)	81.29 [74][a], [58.9][b], [74.1][c]	71.55 [66][d]
c_{44} (GPa)	69.45 [69][a], [67.4][b], [97.8][c]	76.01 [93][d]
A	0.53 [0.39][d]	0.47 [0.42][d]
ζ	0.39	0.33
v	0.27 [0.26][a] , [0.25][d]	0.26 [0.23][d]
H_v (GPa)	10.30	12.83
v_t (m/s)	2898	3337
v_l (m/s)	5194	5844
v_m (m/s)	3201	3678
Θ_D (K)	367.70 [367.60][a]	563.85

[a,b,c]GGA calculations from Refs. [29], [43], [44]; [d]Ref. [27]

The Frantsevich's ratio (*G*/*B*), is routinely used to theoretically gauge if a material is ductile or brittle. A compound is presumed ductile if its G/B value is less than 0.571, otherwise, it is brittle [35]. Accordingly, PtP_2 is predicted to be brittle while PtAs2 is predicted to be a ductile compound. The calculated Zener anisotropy factor (*A*) for the two compounds was less than unity (0.53 and 0.47 respectively). The two compounds possess elastic anisotropy – a result that agrees with earlier predictions (see Table 1). The Kleinman parameter (ζ) value for $PtAs_2$ is 0.39 and 0.33 for PtP_2. ζ, basically describes the ease of bond bending to bond stretching. When ζ = 0, bond bending is lower while bond stretching is higher. Bond stretching is lower, when ζ = 1. With ζ higher in $PtAs_2$ than PtP_2, bond stretching is higher in $PtAs_2$ but lower in PtP_2. The bond strength and type is also a factor that characterizes a material. This can be theoretically gauged using the Poisson's ratio (v), where materials with v ≈ 0.1 are considered to be covalently bonded, those with v ≈ 0.25 are ionic and for metallic bonds, v ≈ 0.33 [45]. The dominant bonding type in $PtAs_2$ and PtP_2 can be predicted to be ionic in nature (where v = 0.27 and 0.26 respectively).

3.2 Phonon Dispersions

The variation of the phonon energy with the q-vector along high symmetry direction of the Brillouin zone is known as the phonon dispersion. Phonon dispersion information can only be experimentally obtained from neutron scattering experiments. As such, phonon dispersion information is available only for limited number of materials. Thus, obtaining theoretical phonon dispersions will help to fill data gaps while it may also serve to establish the validity of a modelling approach. The phonon dispersion curves along high symmetry path for PtP_2 and $PtAs_2$ at zero pressure are shown in Fig. 3(a) & (b). The phonon density of states is shown in Fig. 3(c) & (d). These curves give the macroscopic characterization of the vibrational properties of the materials. Firstly, a material is considered dynamically unstable when phonons of imaginary frequencies are present over much of its path in the Brillouin zone. Therefore, PtP_2 and $PtAs_2$ are dynamically stable as evidently shown in Figs. 3 (a) & (b), where phonons of negative frequencies are absent in the plots. The glitches at the Γ point in Fig. 3(b) are not phonons of imaginary frequencies but numerical errors or fluctuations arising from the minimization method used to compute the phonons, which is considered normal in this type of calculation. However, the low frequency acoustic modes, associated with bond bending is predicted to be between 100 - 170 cm^{-1} for $PtAs_2$ (Fig. 3 (c)) while it is 100 - 190 cm^{-1} for PtP_2 (see Fig. 3 (d)). The high frequency transverse optical (TO) can be predicted to be 410 cm^{-1} for PtP_2 while it is 250 cm^{-1} for $PtAs_2$. When the phonon density of states (Fig. 3 (c) & (d)) are further compared, it can be concluded that the reduction in the height of the peak of the high frequency (TO) of PtP_2 would lead to additional bond-bending modes in PtP_2 than in $PtAs_2$.

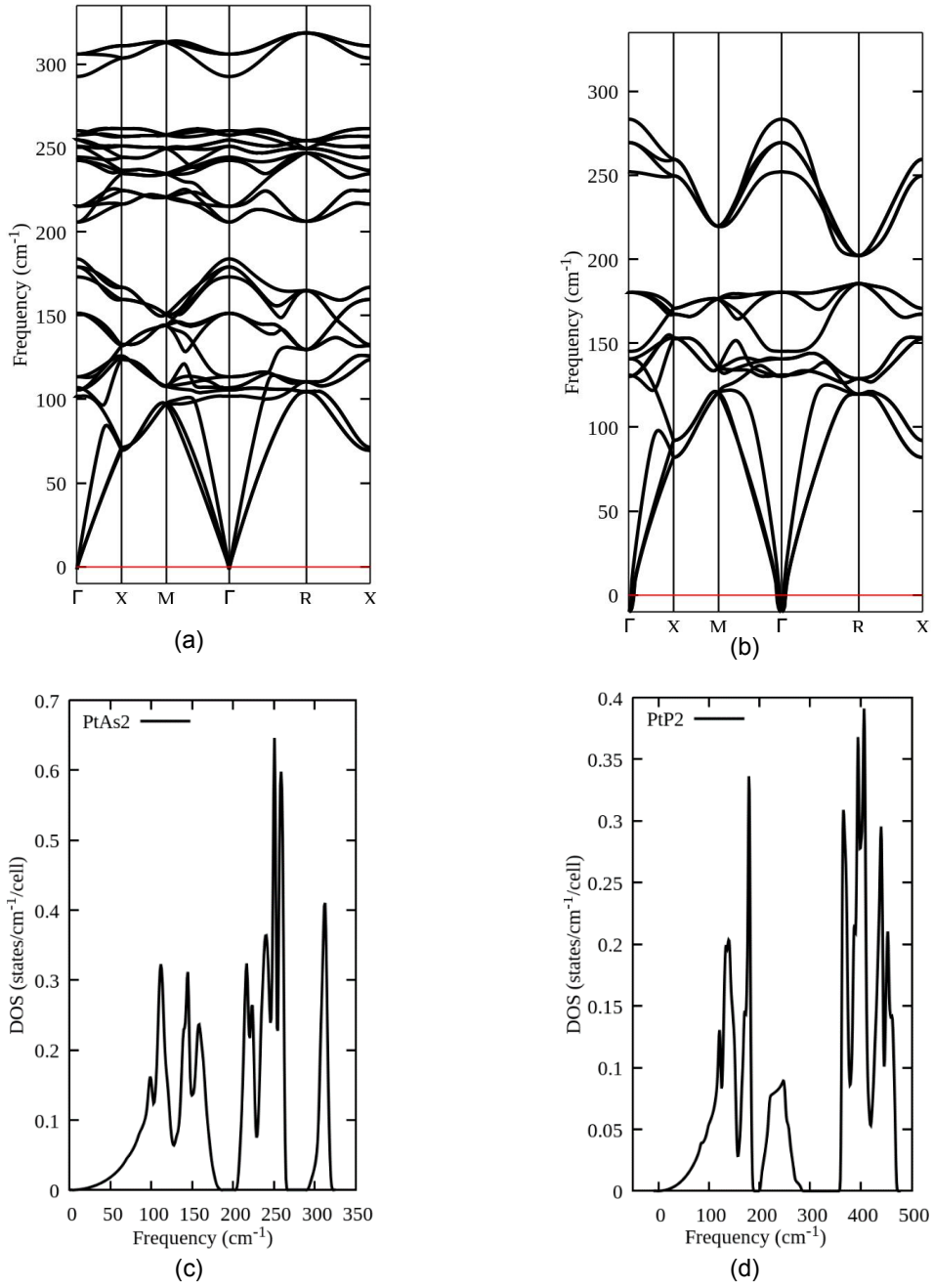

Fig. 3. Calculated phonon band structure and density of states; (a) $PtAs_2$ phonon dispersion; (b) PtP_2 phonon dispersion; (c) phonon density of states for $PtAs_2$; (d) phonon density of states for PtP_2

3.3 Thermodynamic Properties

There are connections between the thermodynamic properties of a material, its electronic structure and the elastic moduli. It therefore becomes necessary to investigate the thermodynamic performance of a material to have a deeper knowledge on it under extremely conditions. As an example, the Debye temperature, relates with the specific heat, dynamic properties, and the melting temperature of solids. It is under these considerations that the thermodynamic properties of $PtAs_2$ and PtP_2 were evaluated. The result for the entropy, free

energy and the specific heat capacity at constant volume are given in Fig. 4. According to Fig. 4(a), $PtAs_2$ will experience higher entropy compared to PtP_2. The entropy which increases with temperature is predicted to have a value of 264.18 J/K for PtP_2 and 354.51 J/K for $PtAs_2$ at 300 K respectively. The thermal stability of any material is related to the entropy. The vibration free energy of $PtAs_2$ is smaller (see Fig. 4(b)) compared to that of PtP_2. Thus, PtP_2 has more internal energy, available for work than PtP_2. The specific heat capacities at constant volume for the compounds are given in Fig. 4(c). A constant value of about 293 J/K is predicted for $PtAs_2$ and 284 J/K for PtP_2 at 300 K respectively. Within the considered temperature range (0 to 800 K), $PtAs_2$ demonstrated higher specific heat capacity than PtP_2 and hence, more work would need to be done for charge carriers to be liberated in $PtAs_2$ than in PtP_2.

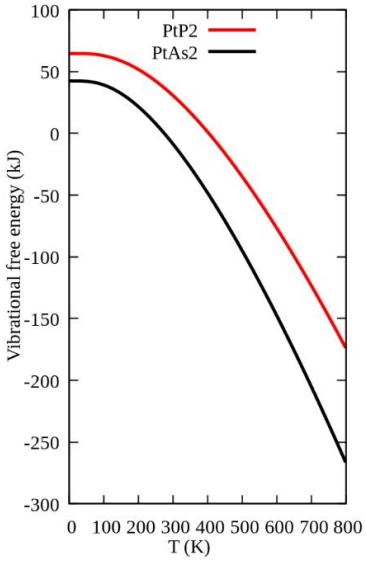

(a)

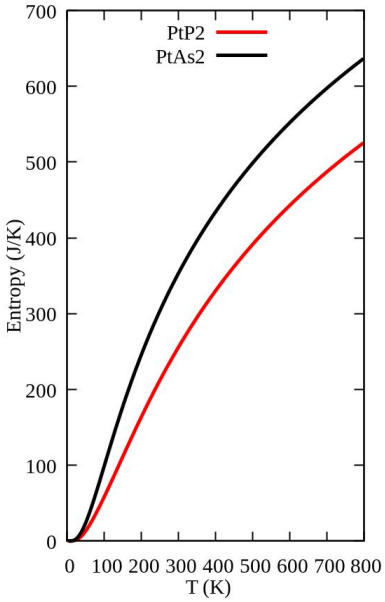

(b)

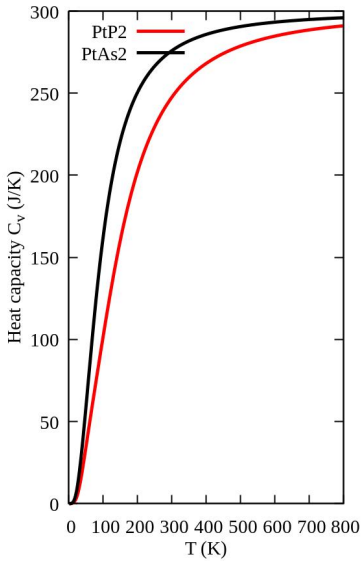

(c)

Fig. 4. Calculated; (a) free energy; (b) entropy; (c) heat capacity for $PtAs_2$ and PtP_2

4. CONCLUSION

$PtAs_2$ and PtP_2 are semiconductors with similar crystal and electronic structures. Both have been proposed for thermoelectric application. The transport properties such as the Seebeck coefficient and the power factor of PtP_2 had been predicted much higher than that of $PtAs_2$ and this has been attributed to the wider band gap of PtP_2. This investigation used the *ab-initio* calculation method to evaluate the elastic, vibration and the thermodynamic behaviour of $PtAs_2$ and PtP_2. This was done to understand the role of these practical oriented properties *vis-à-vis* band gap size on the thermoelectric properties of $PtAs_2$ and PtP_2. The calculated mechanical and thermodynamic properties conferred better performance on PtP_2 over $PtAs_2$. The phonon dispersion showed stronger/higher bond bending in PtP_2 than $PtAs_2$. The hybridization of Pt (electronic structure = [Xe] $4f^{14}$ $5d^9$ $6s^1$) d-states with lower level valence states in phosphorus ([Ne] $3s^2$ $3p^3$) could have led to PtP_2 exhibiting higher bond bending than in $PtAs_2$, where the hybridization is between the Pt d-states and higher arsenic ([Ar] $3d^{10}$ $4s^2$ $4p^3$) valence states. It can thus be concluded that in the process of designing optimum thermoelectric materials, hybridization between the d-orbital of a transition metal and the lower valence states of a metalloid or non-metallic element would play a significant role and phonon dispersion can be sufficiently used to identify material with higher thermopower.

ACKNOWLEDGEMENT

The authors would like to thank the Department of Physics, the Federal University of Technology, Akure (FUTA) for providing the back-up power supply during the computations.

COMPETING INTERESTS

Authors have declared that no competing interests exist.

REFERENCES

1. Ozturk S, Sozdemir A, Ulger O. The real crisis waiting for the world: Oil problem and energy security. International Journal of Energy Economics and Policy. 2013;74–79.
2. Bhattarai K, Stalick WM, Mckay S, Geme G, Bhattarai N. Biofuel: An alternative to fossil fuel for alleviating world energy and economic crises," Journal of Environmental Science and Health. 2011;46(12):1424–1442.
3. Zheng JC. Recent advances on thermoelectric materials. Frontiers of Physics in China. 2008;3(3):269–279.
4. Yang J. Potential applications of thermoelectric waste heat recovery in the automotive industry. Proceedings of the 24th IEEE International Conference on Thermoelectrics. 2005;170–174.
5. Matsubara K. Development of a high efficient thermoelectric stack for a waste exhaust heat recovery of vehicles. Proceedings of the IEEE 21st International Conference on Thermoelectrics. 2005;418–423.
6. Gilley MD, Webb RL. Thermoelectric refrigerator with evaporating/condensing heat exchanger; 1999.
7. Putra N. Design, manufacturing and testing of a portable vaccine carrier box employing thermoelectric module and heat pipe. Journal of medical engineering and Technology. 2009;33(3):232–237.
8. Harman T, Taylor P, Walsh M, La Forge B. Quantum dot superlattice thermoelectric materials and devices. Science. 2002;297(5590):2229–2232.
9. Belton JJF, Leo S. Thermoelectric air conditioning apparatus. US Patent. 1960;2949014.
10. Newton AB. Thermoelectric air conditioning systems. US Patent. 1996;3252504.
11. Xi L, Yang J, Wu L, Yang J, Zhang W. Band engineering and rational design of high-performance thermoelectric materials by first-principles. Journal of Materiomics. 2016;2(2):114.
12. Snyder GJ, Toberer ES. Complex thermoelectric materials, in materials for sustainable energy: A collection of peer-reviewed research and review articles from Nature Publishing Group, World Scientific. 2011;101–110.
13. Shakouri A. Recent developments in semiconductor thermoelectric physics and materials. Annual review of materials research. 2011;41.
14. Kuroki D, Arita R. Pudding mold-type band dispersion as the origin of large thermo-power in Na_xCoO_2. Journal of the Physical Society of Japan. 2007;76:083707.
15. Yang HB, Wang SC, Sekharan AKP, Matsui H, Souma S, Sato T, et al. ARPES on $Na_{0.6}CoO_2$: fermi surface and unusual

band dispersion. Physical Review Letters. 2004;92:6403.

16. Terasaki I, Sasago Y, Uchinokura K. Large thermoelectric power in $NaCo_2O_4$ single crystals. Physical Reviews B. 1997;56:R12685.
17. Motohashi T, Naujalis E, Ueda R, Isawa K, Karppinen M, Yamauchi H. Simultaneously enhanced thermoelectric power and reduced resistivity of $Na_xCo_2O_4$ by controlling Nanonstoichiometry. Applied Physics Letters. 2001;79(10):1480-1482.
18. Okamoto Y, Nohara M, Sakai F, Takagi H. Correlated metallic phase in a doped band insulator $Sr_{1-x}Rh_2O_4$. Journal of the Physical Society of Japan. 2006;023704:75.
19. Arita R, Kuroki K, Held K, Lukoyanov AV, Skornyakov S, Anisimov VI. Origin of large thermopower in $LiRh_2O_4$: Calculation of the Seebeck coefficient by the combination of local density approximation and dynamical mean-field theory. Physical Review B. 2008;78(11):115121.
20. Usui H, Arita R, Kuroki K. First-principles study on the origin of large thermopower in hole-doped $LaRhO_3$ and $CuRhO_2$. Journal of Physics: Condensed Matter. 2009;21(6):4223.
21. Mori K, Usui H, Sakakibara H, Kuroki K. Theoretical expectation of large Seebeck effect in $PtAs_2$ and PtP_2. Journal of the Physical Society of Japan. 2014;83(2):023706.
22. Nishikubo Y, Nakano S, Kudo K, Nohara M. Enhanced thermoelectric properties by Ir doping of $PtSb_2$ with pyrite structure. Applied Physics Letter. 2012;100:252104.
23. Kudo K, Nakano S. Mizukami T. Takabatake T. Nohara M. Enhancing high-temperature thermoelectric properties of $PtAs_2$ by Rh doping. Appl. Phys. Lett. 2013;103:092107.
24. Casado-Rivera E, Gal Z. Ângelo ACD. Lind C. DiSalva FJ. Abruna HD. Electrocatalytic activity of ordered intermetallic phases for fuel cell applications. Journal of the American Chemical Society. 2004;126(12):4043–4049.
25. Innocente AF, Ângelo ACD. Electrocatalysis of oxidation of hydrogen on platinum ordered intermetallic phases. Kinetic and mechanistic studies. Journal of Power Sources. 2006;162:151-159.
26. Zhang L, Xia D. Electrocatalytic activity of ordered intermetallic PtSb for methanol electro-oxidation. Appl. Surf. Sci. 2006;252:2191-2195.
27. de Jong M, Chen W, Angsten T, Jain A, Notestine R, Gamst A, et al. Charting the complete elastic properties of inorganic crystalline compounds. Scientific Data 2. 2015;150009.
DOI:10.1038/sdata.2015.9
28. Ivano E, Castelli FH, Mohnish P, Hong Li, Kristian S, Thygesen BS, Anubhav J, Kristin P, Gerbrand C, Karsten WJ. New light harvesting materials using accurate and efficient bandgap calculations. Advanced Energy Materials; 2014.
DOI: org/10.1002/aenm.20140091
29. Haiyan Y, Meiguang Z. Theoretical investigation on compressibility, electronic and thermodynamic properties of single crystal $PtAs_2$ under high pressure. Computational Materials Science. 2014;86:124–129.
30. Ricci F, Chen W, Aydemir U, Snyder GJ, Rignanese GM, Jain A. Hautier G. Data descriptor: An ab initio electronic transport database for inorganic materials. Scientific Data. 2017;4:170085.
DOI: org/10.1038/sdata.2017.85
31. Kokalj A. Computer graphics and graphical user interfaces as tools in simulations of matter at the atomic scale, Comp. Mater. Sci. 2003;28:155-168.
32. Giannozzi P, Baroni S, Bonini N, Calandra M, Car R, Cavazzoni C, et al. Quantum espresso: A modular and open-source software project for quantum simulations of materials. Journal of Physics Condensed Matter. 2009;21(39):21395502.
33. Perdew JP, Burke K, Ernzerhof M. Generalized gradient approximation made simple. Physical Review Letters. 1996;77(18):3865–3868.
34. Monkhorst HJ, Pack JD. Special points for Brillouin-zone integrations. Phys. Rev. 1976;B13:5188.
35. Papaconstantopoulos DA, Mehl MJ. Tight binding method in electronic structure. Encyclopedia of Condensed Matter Physics, Elsevier B.V; 2005.
36. Hill R. The elastic behavior of a crystalline aggregate. Proceedings of the Physical Society. 2005;65:349-354.
37. Zener C. Elasticity and inelasticity of metals. University of Chicago Press; 1948.
38. Güler E, Güler M. Phase transition and elasticity of gallium arsenide under pressure. Materials Research. 2014;17(5):1268-1272.

39. Chen XQ, Niu H, Li D, Li Y. Modeling hardness of polycrystalline materials and bulk metallic glasses. 2011;19(9):1275-1281.
40. Anderson OL. A simplified method for calculating the Debye temperature from elastic Constants. Journal of Physics and Chemistry of Solids. 1963;24(7):909-917.
41. Baroni S, De Gironcoli S, Dal Corso A, Giannozzi P. Phonons and related crystal properties from density-functional perturbation theory. Reviews of Modern Physics. 2001;73:515–562.
42. Mouhat F, Coudert FX. Necessary and sufficient elastic stability conditions in various crystal systems. Physical Reviews B. 2014;90(22):224104.
43. Oliver T, Boris K, Florent T, Kimberly T, Judith B, Andreas Z, Przemyslaw D, Alastair M, Jason K, Simon C. Elastic moduli and hardness of highly incompressible platinum perpnictide $PtAs_2$. Applied Physics Letters 103,101901; 2013.
44. Ngoepe PE, Ntoahaea PS, Mangwejanea SS, Sithole HM, Parker SC, Wright KV, de Leeuw NH. Atomistic simulation studies of iron sulphide, platinum antimonide and platinum arsenide. South African Journal of Science. 2005;101:480–483.
45. Tariq S, Ahmed A, Saad S, Tariq S. Structural, electronic and elastic properties of the cubic CaTiO under pressure: A DFT study. AIP Advances. 2015;5(7): 077111.

Peer-review history:
The peer review history for this paper can be accessed here:
http://www.sdiarticle4.com/review-history/68465